Supporting Information: A Composite Microwave Cavity for Liquid Volume Fraction and Simultaneous Phase Permittivity Measurements

Liam D. Tenardi [a, c], Matthew G. Hopkins [a, c], Markus Richter [a, b, c], Eric F. May [a, c], and Paul L. Stanwix [a, c]*

[a] Fluid Science & Resources Division, School of Engineering, The University of Western Australia, Crawley, WA 6009, Australia

[b] Applied Thermodynamics, Faculty of Mechanical Engineering, Chemnitz University of Technology, 09107 Chemnitz, Germany

[c] Future Energy Exports Cooperative Research Centre, Crawley, WA 6009, Australia

* Corresponding author

Email address: paul.stanwix@uwa.edu.au (Paul L. Stanwix)

Table of Contents

1. PEEK Dielectric Property Measurements

The dielectric constant for the PEEK supplied by the manufacturer was specified to be 3.2 based on an IEC 60250 test [1]. However, they state that this is only a guideline. In an effort to improve the PEEK-fluid characterisation, the dielectric constant for the PEEK used in the MRVLE was measured with a cylindrical resonator. As shown in Figure 1 (a), a piece of PEEK was machined to entirely fill the cylindrical cavity, with two holes bored to a depth of 3 mm to allow for coupling with the antennae. When assembled, as shown in Figure 1 (b), the PEEK sits flush within 0.1 mm of the base, wall, and lid, taking up the entire volume of the cylinder. A port in the cylinder enabled the cell to be evacuated with and without the PEEK inside to remove impurities. Furthermore, microwave feedthrough antennae were used with high pressure fittings to seal the cell.

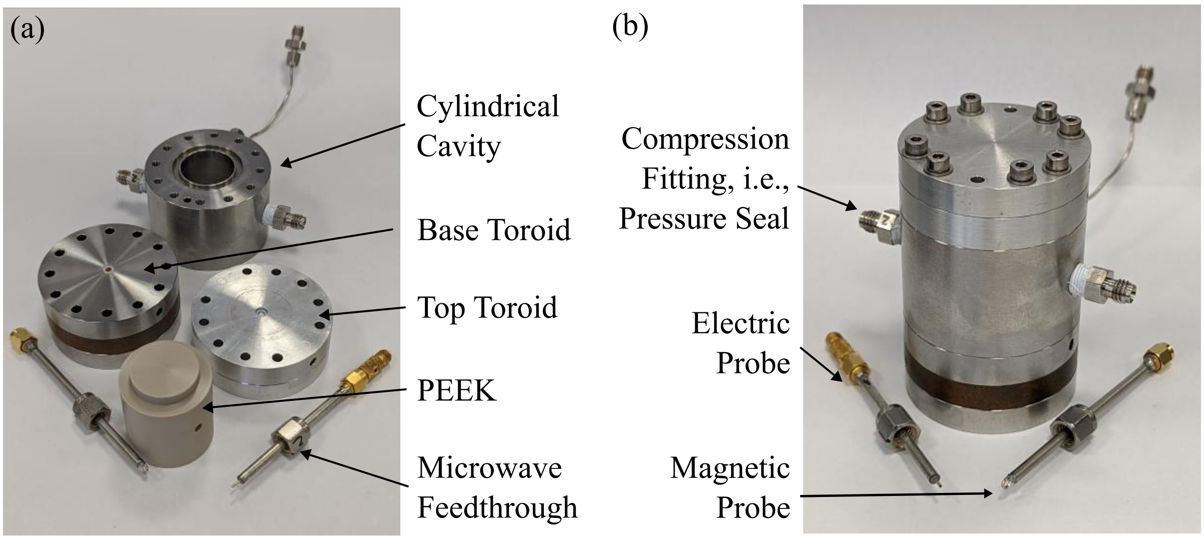

Figure 1. Concept composite cavity used to measure dielectric constant of PEEK. (a) exploded view of the cell showing the PEEK block with antennae holes, and (b) is the assembled cavity.

Four resonance frequencies exist in the range of the vector network analyser (VNA) (Hewlett Packard, 8719ET) from (0 to 11) GHz. Mode 1 is an azimuthal mode with simulated resonance at 6.383 GHz, mode 2 is non-azimuthal at 6.666 GHz, mode 3 is non-azimuthal at 7.976 GHz, and finally mode 4 is azimuthal at 9.218 GHz. The azimuthal modes were coupled to effectively with an electric probe and a magnetic probe. These modes are displayed in Figure 2 and were chosen to centre the electric field within the PEEK and minimise any contribution of the antenna bores or gaps in the edges on measured frequency. Measured vacuum resonance frequencies for these two modes are 6.378 GHz for mode 1 and 9.191 GHz for mode 4 at 293 K and were characterised as a function of temperature.

(a) (b)

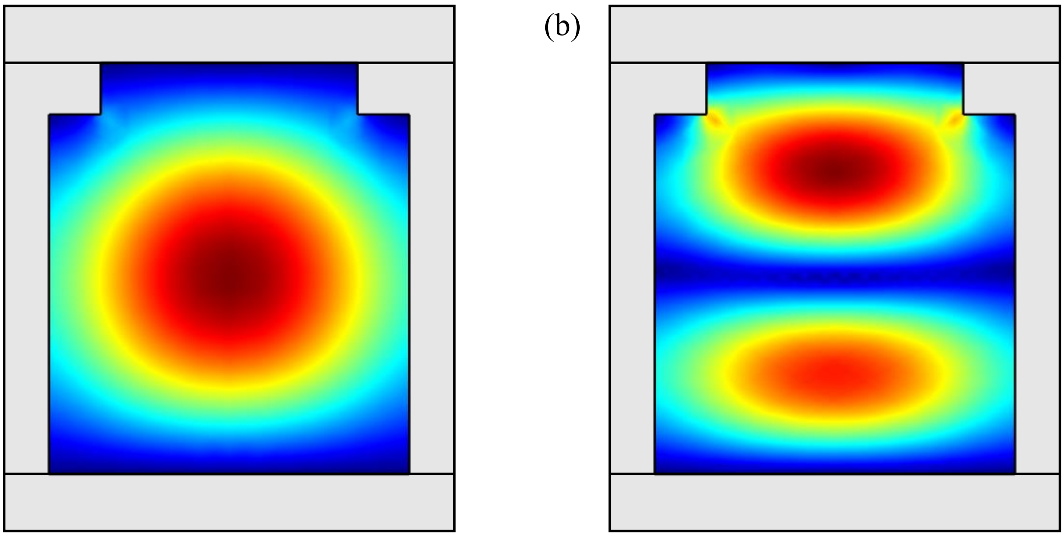

Figure 2. Azimuthal modes tracked in measuring the dielectric constant of PEEK: (a) mode 2 at 6.666 GHz, and (b) mode 4 at 9.218 GHz.

The dielectric constant of PEEK was measured over a temperature range of (213 to 353) °K. Results for both modes are plotted in Figure 3, with two measurement sets taken a year apart. There appears to be a temperature dependence in each mode, with each decreasing in temperature. However, as the PEEK is incompressible and rigid, thermal contraction may not be uniform around the cell and change the vacuum frequency from what was measured without the PEEK. Furthermore, each measurement required disassembling and assembling the resonator to remove the PEEK. Different torquing of the bolts on the cavity between vacuum and PEEK measurements or orientations of the PEEK could affect the vacuum frequency and influence the dielectric constant measurement. Results suggest a frequency dependence on the dielectric constant of PEEK following an inverse relationship. As all modes in the MRVLE are below 6.378 GHz, the dielectric constant of mode two was considered to be the PEEK dielectric constant for the MRVLE. The original estimation for the real component of the dielectric constant of PEEK was 3.16 and was used throughout the work.

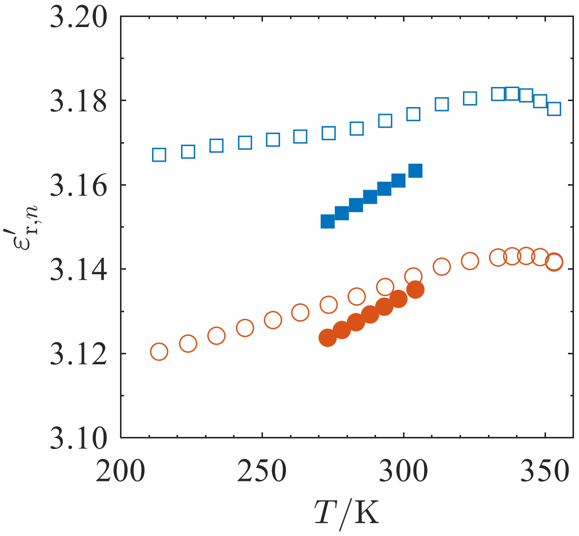

Figure 3. Real component of the dielectric constant ε_r' of PEEK, measured by the n modes as a function of temperature T. Modes 2 (□) at 6.355 GHz and 4 at 9.191 GHz (○) were measured a year after the first measurements (■, ●) respectively.

2. Characterisation of $G_n^{(\mathrm{VLE})}(\gamma_n^{(\mathrm{VLE})})$

Similar to the electric field distribution between the fluid and PEEK interface, the electric field distribution between a vapour and liquid phase depends on the fluid properties. Hopkins et al. [2] characterised variations in $G_n^{(\mathrm{VLE})}$ (formerly G_n) due to an impedance mismatch at the vapour-liquid interface with the ratio $\gamma_n^{(\mathrm{VLE})} = (\varepsilon_L/\varepsilon_V)$ (formerly γ). A similar behaviour was observed with the MRVLE. However, this system is more complicated with the inclusion of the PEEK inserts, so a rigorous finite element analysis of the effects of $\gamma_n^{(\mathrm{VLE})}$ on $G_n^{(\mathrm{VLE})}$ was performed. Figure 4 shows the electric field distribution of the cavity mode for (a) a vacuum $\gamma^{\mathrm{VLE}} = 1$ and (b) for an arbitrary fluid $\gamma^{\mathrm{VLE}} = 2$ at a liquid volume fraction (Λ) of 0.5. With a higher $\gamma_n^{(\mathrm{VLE})}$ more of the electric field is concentrated in the vapour phase, pulling it from the liquid phase and PEEK insert.

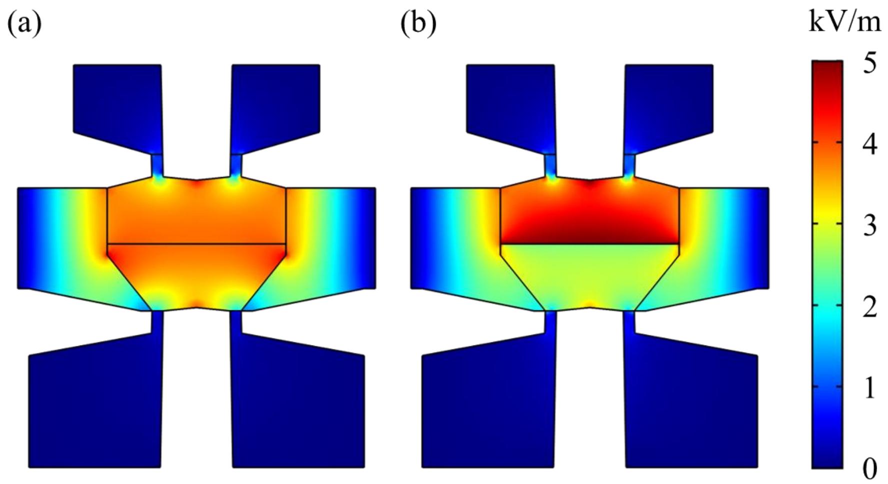

Figure 4. Normalised electric field distribution of the cavity mode for (a) a vacuum where $\gamma_n^{(\mathrm{VLE})}$ = 1, and (b) for an arbitrary fluid in vapour-liquid equilibrium with $\gamma_n^{(\mathrm{VLE})}$ = 2. Both electric fields are referenced to the same colour scale.

Characterisation of the field distribution was achieved by simulating the mode shape for different values of $\gamma_n^{(\mathrm{VLE})}$. Figure 5 demonstrates the value $G_n^{(\mathrm{VLE})}$ can take for $\gamma_n^{(\mathrm{VLE})}$ ranging from 1.2 to 2.4 for each mode. Subfigures (a), (c) and (e) are the mode shape plots of the top, cavity, and base modes respectively, and likewise, subfigures (b), (d) and (f) are deviations plots of the mode shapes from $\gamma_n^{(\mathrm{VLE})}$ = 1.6. The top mode begins to deviate most at high Λ, when the liquid enters the fringing field. Similarly, the base mode deviates most at low Λ until most of the fringing field is covered. However, these occur outside of the operating region of the resonator, so for low dielectric constant fluids this effect will have little effect on the phase permittivities after inversion. The cavity mode deviates the most of all modes, especially in the operating range of the resonator. It is therefore important to use a mode shape closest to the γ^{VLE} of the measured fluid to ensure accurate liquid volume fraction measurements.

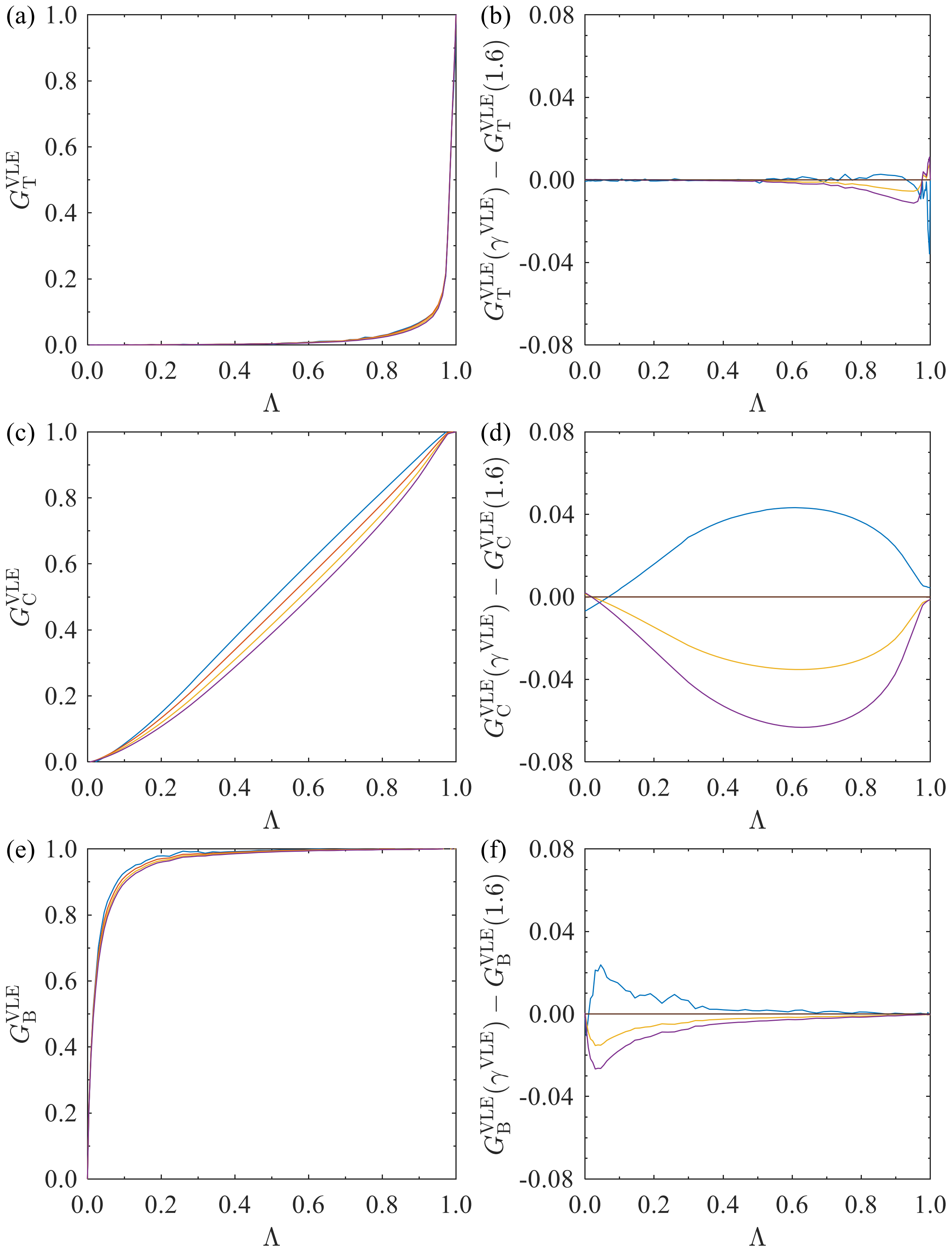

Figure 5. Simulation of the mode shape $G_n^{(\mathrm{VLE})}$ response to liquid volume fraction Λ for cases where $\gamma_n^{(\mathrm{VLE})}$ is equal to 1.2 (—), 1.6 (—), 2.0 (—), and 2.4 (—). The n modes are displayed separately for (a) the top mode, (c) cavity mode, and (e) base mode. Deviations of each case of $\gamma_n^{(\mathrm{VLE})}$ from $\gamma_n^{(\mathrm{VLE})}$ = 1.6 are plotted for the respective modes in (b), (d), and (f).

The electric field distribution was investigated for fluids with the same $\gamma_n^{(\mathrm{VLE})}$. In Figure 6, $\gamma_n^{(\mathrm{VLE})}$ is 1.6 for both plots; however, the liquid dielectric constant in (a) is 1.6 and in (b) is 2.4. There are some subtle differences between the cases. Firstly, the electric field within the PEEK is weaker in (b). Secondly, the electric field is stronger in the liquid at the tip of the post from the base toroid in (b). These effects also need to be accounted for.

Figure 7 demonstrates the effect of fluids with the same $\gamma_n^{(\mathrm{VLE})}$ but varying phase dielectric constants on the mode shape. (a), (c), and (e) represent the mode shapes of the top, cavity, and base modes respectively. (b), (d), and (f) show the deviation in mode shape from the reference case where the dielectric constant of the liquid phase is 1.6. The top mode has deviations much less than 0.01 between mode shapes across the whole liquid volume fraction range. However, the base mode has larger deviations, staying around 0.01 for the Λ range to 0.8. The trend shows that as the liquid dielectric constant increases, the mode shape separates further. Finally, the cavity mode shows a change in the geometry of the mode shape with varying liquid dielectric constant. Therefore, a new methodology is needed to produce the mode shapes for the inversion function than the 3D spline proposed by Hopkins et al. [2].

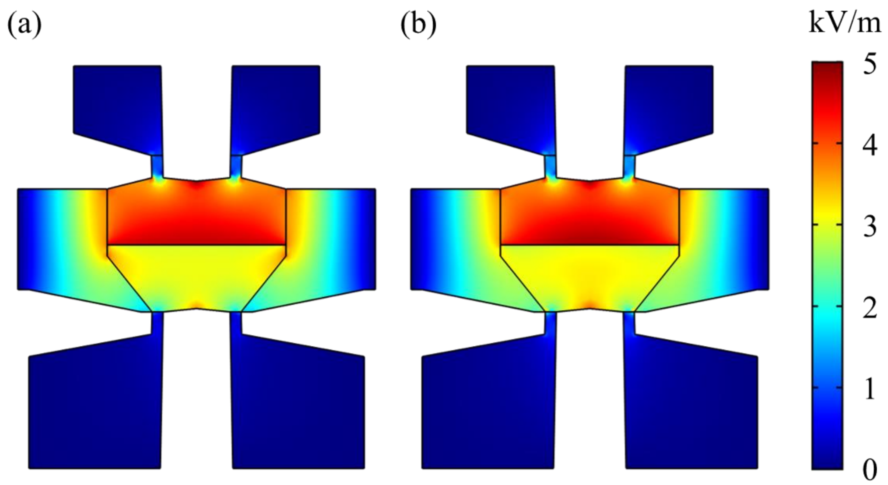

Figure 6. Normalised electric field distribution of the cavity mode where $\gamma_n^{(\mathrm{VLE})}$ = 1.6 in both cases. However, the liquid dielectric constant in (a) is 1.6, and in (b) is 2.4. Both electric fields are referenced to the same colour scale.

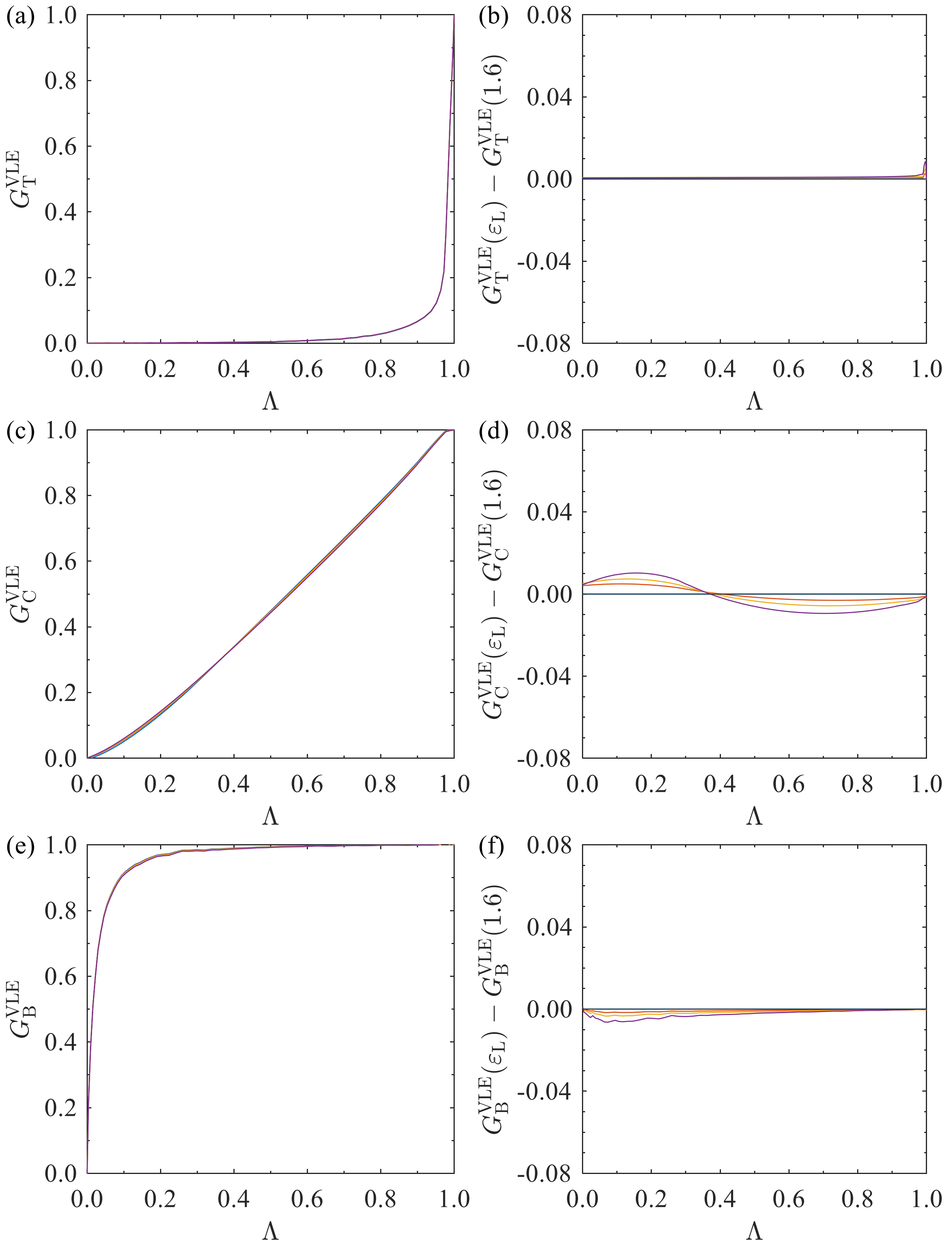

Figure 7. Simulation of the mode shape $G_n^{(\mathrm{VLE})}$ response to liquid volume fraction Λ where γ_n^{VLE} = 1.6 for all modes. However, the liquid dielectric constant ε_{L} is varied for cases equal to 1.6 (—), 1.8 (—), 2.0 (—), and 2.4 (—). The n modes are displayed separately for (a) the top mode, (c) cavity mode, and (e) base mode. Deviations of each case from ε_{L} = 1.6 are plotted for the respective modes in (b), (d), and (f).

3. MRVLE Volume Calibration

It is important to understand the volume characteristic of the apparatus for accurate liquid volume fraction measurements. The microwave resonator can only measure liquid volume fraction of the sample space and cannot detect phases of the dead volume. Figure 8 illustrates these regions of sample space and dead volume within the apparatus. Dead volume above the cell starts at valve 1, passes through the tubing, pressure transducer, and terminates at the end of the top fluid port. Similarly, dead volume below the sample space starts at valve 2, passes through the tubing, and terminates at the end of the bottom fluid port. The remainder of what is highlighted is the sample space, which is the region that interacts with the electromagnetic field. A set of injection measurements were carried out with methane and propane to determine the volumes of each region.

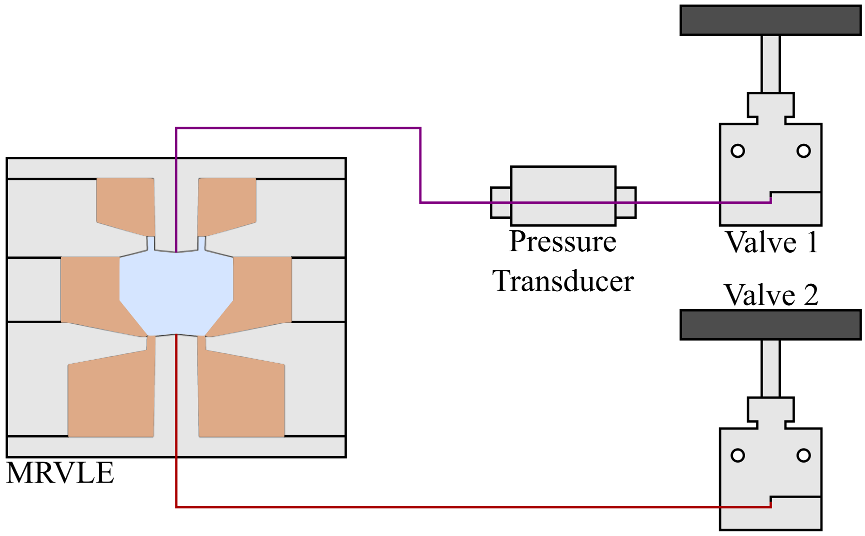

Figure 8. Cross-section of the measurement cell volume, approximately 2.05 mL at 6 MPa. The sample space (■) has a volume of 1.95 mL, dead volume above the cell (■) is 0.04 ml, and dead volume below the cell (■) is 0.06 mL.

The total cell volume was determined through injection measurements with methane. Initially the sample space was evacuated from valve 1 to 2 in Figure 8. A syringe pump was pressurised with methane and connected to valve 2. The p-T-V conditions of the syringe pump were recorded prior to the methane injection to calculate the number of moles in the pump from the equation of state (EOS) as implemented in REFPROP 10.0 [3, 4]. Valve 1 was closed and 2 opened to transfer the methane into the sample space, before closing valve 2. Again, the p-T-V conditions of the syringe pump were used to calculate the moles in the syringe pump after the injection. Furthermore, the p-T conditions of the cell were used to estimate the density with the same EOS [3, 4]. Finally, the volume was estimated from the moles transferred and cell density.

Volume measurements were conducted over a range of cell pressures from (2 to 8) MPa and temperatures from (283 to 296) K. Figure 9 shows the results of the measurements as: (a) a function of pressure, and (b) a function of temperature. There appeared to be a trend of increasing volume with pressure, which was expected behaviour for a pressure vessel. Furthermore, there was a gradual slope with increasing temperature in the cell volume. Over the p-T range, the trend was within the scatter of the measurements and assumed to be within the uncertainty of the volume measurement. A value of 2.05 mL was selected to be the volume of the apparatus between valves 1 and 2 in Figure 8, which was the average value of measurements at 6.0 MPa.

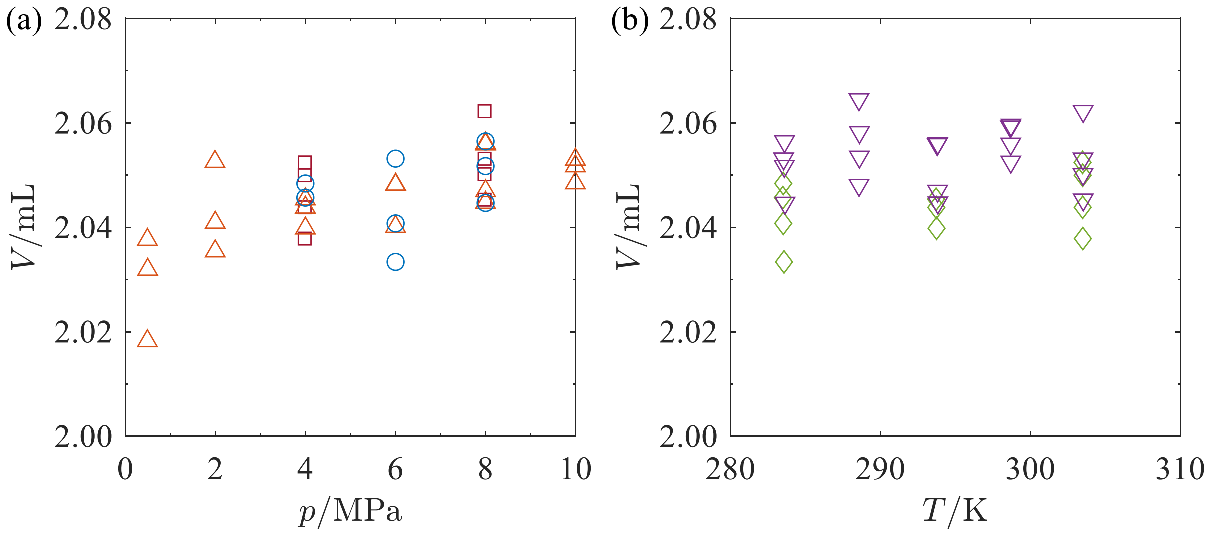

Figure 9. Measurements of total cell volume (V), occupying all the fluid area between the valves in Figure 8. (a) displays this as a function of pressure p, for 303 K (□), 293 K (△), and 283 K (○). (b) Displays this as a function of cell temperature T, for measurements at 4 MPa (◇), and 8 MPa (▽).

The total volume of 2.05 mL comprises of three regions, shown in Figure 8: the sample space; dead volume above the cell, including the injection port, tubing, pressure transducer, and the valve; and the dead volume below the cell, including the injection port, tubing, and valve. Both dead volumes were measured to determine the volume of each of the regions.

Dead volume below the cell was measured by pushing a liquid into the cavity and measuring the frequency as a function of injection volume. The cell was pressurised with methane vapour to 2 MPa through valve 1. A syringe pump containing propane liquid at 2 MPa was attached to valve 2. Liquid was pushed through valve 2 at a rate 0.01 mL·min^{-1} until a change in resonant frequency was noticed in the base mode. As displayed in Figure 10 (a), the frequency changed after 0.06 mL was injected. Therefore, the dead volume below the cell was estimated to be 0.06 mL.

Similarly, the dead volume above the cell was measured by pushing a gas into the cavity and measuring the frequency as a function of injection volume. The cell was pressurised with propane liquid to 2 MPa from valve 2. A syringe pump pressurised with methane vapour to 2 MPa was attached to valve 1. The vapour was pushed through the resonator at 0.01 $mL \cdot min^{-1}$ and continued until the first bubbles were detected by the top mode. The results are shown in Figure 10 (b), with the dead volume above the cell estimated to be 0.04 mL. Therefore, the total volume of the sample space was estimated to be 1.95 mL by subtracting the dead volume from the total volume, agreeing with the FEA simulation for sample space volume of 1.95 mL.

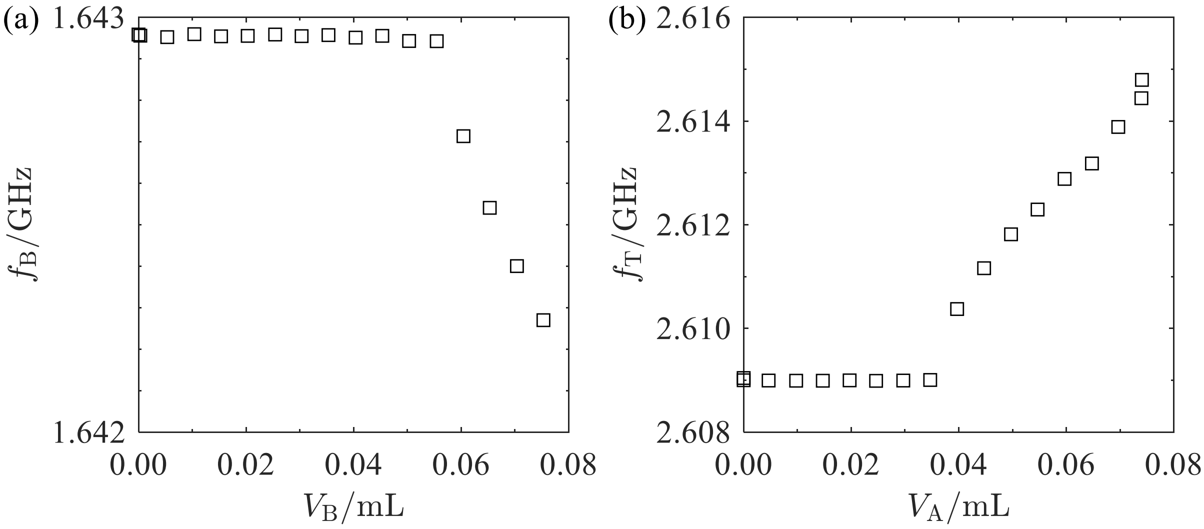

Figure 10. (a) Frequency of the base mode f_B as a function of liquid propane volume injected below the resonator V_B. (b) Frequency of the top mode f_T as a function of methane vapour volume injected above the resonator V_A.

4. References

1. Röchling, (Röchling Industrial Lahnstein SE & Co. KG, Lahnstein, Germany 2023),
2. M.G. Hopkins, Y. Leusmann, M. Richter, E.F. May, P.L. Stanwix, Journal of chemical and engineering data 65 (7), 3393 (2020) doi:https://doi.org/10.1021/acs.jced.0c00213
3. U. Setzmann, W. Wagner, Journal of Physical and Chemical Reference Data 20 (6), 1061 (1991) doi:https://doi.org/10.1063/1.555898
4. E.W. Lemmon, I.H. Bell, M.L. Huber, M.O. McLinden, (2018) doi:https://doi.org/10.18434/T4/1502528